J Appl Electrochem (2014) 44:447–453
DOI 10.1007/s10800-013-0634-2

RESEARCH ARTICLE

On the electrochemical activation of alkali-treated soft carbon for advanced electrochemical capacitors

Masayuki Morita · Ryo Arizono · Nobuko Yoshimoto · Minato Egashira

Received: 27 July 2013 / Accepted: 4 October 2013 / Published online: 17 October 2013

Abstract The electrochemical activation process of the so-called "alkali-treated soft carbon" (ASC) has been examined in organic electrolyte solutions. SEM observation demonstrated that the edge plane of graphene structure of the ASC particle becomes rough after the activation, and XRD measurements indicated that the average lattice constant of graphene stacking in ASC increases after the activation process. Ex-situ ^{7}Li NMR measurements proved that the insertion of cation (Li^{+}) into the pore structure of ASC is associated with the activation process in the electrolyte dissolving Li salt. The pore-size distribution determined from N_2-gas adsorption for ASC electrodes before and after the electrochemical activation indicates that the pore structure becomes developed after the electrochemical polarization, especially in the pore-diameter range of 2–10 nm. A schematic model of the activation process has been presented, which includes electrochemical insertion of ions into the inside of the ASC.

Keywords Soft carbon · Capacitor · Electrochemical activation · Ion insertion

Presented at 3rd International Symposium on Enhanced Electrochemical Capacitors (ISEECap 2013), Taormina, Italy.

M. Morita (✉) · R. Arizono · N. Yoshimoto · M. Egashira
Graduate School of Science and Engineering, Yamaguchi University, 2-16-1 Tokiwadai, Ube 755-8611, Japan
e-mail: morita@yamaguchi-u.ac.jp

Present Address:
M. Egashira
College of Bioresource Sciences, Nihon University, 1866 Kameino, Fujisawa 252-0880, Japan

1 Introduction

Various types of carbon materials with high specific surface area have so far been used as the electrodes of electric double-layer capacitors (EDLCs) [1, 2]. These have different types of porous structures depending on the raw material and preparation conditions. Recently, carbon materials with ordered pore structures have been proposed as high-rate performance electrodes in organic electrolyte solutions [3–5]. Besides these, non-porous carbon materials having rather moderate surface area ($<100\ m^2\ g^{-1}$) can also be applied to EDLC, which show high capacitive currents after proper electrochemical treatments [6–9]. This type of carbon has originally been named as "Nano-gate Carbon," and later called Alkali-treated Soft Carbon (ASC), considering the raw material and the preparation procedure. It shows characteristic behavior of high specific capacitance per volume ($F\ L^{-1}$) after the treatment of the so-called "electrochemical activation."

We have previously reported on an advanced hybrid capacitor that uses ASC as the positive electrode and conventional hard carbon as the negative electrode with an organic electrolyte solution [10]. The advanced capacitor system realizes much higher energy density and power density per volume than those of conventional EDLCs using activated carbon electrodes. Higher specific capacitance and higher operation voltage, which can be achieved for this electrode combination, result in such excellent performances.

During the course of developing the advanced capacitor using ASC, we found that the electrochemical activation of ASC depends not only on the polarization conditions but also on the electrolyte composition (solvent and salt) [11, 12]. That is, different activation conditions cause different capacitor performances of ASC. Thus, in this work, we have focused on the electrochemical activation of ASC

itself. Changes in the morphology, crystallographic and pore structures, and the chemical state of adsorbed species during or after the electrochemical activation of ASC in an organic solution dissolving a lithium salt were investigated using spectroscopic methods (SEM, Raman, XRD, and ^{7}Li NMR) and N_2-gas adsorption/desorption measurements. From these observations, the electrochemical process at ASC electrode during the activation is discussed in detail.

2 Experimental

The sample ASC (received from Daihatsu Motor Co. Ltd.) was prepared from aromatic resin, which was carbonized and heat-treated with KOH at 800 °C [10]. It was further treated by heating in a vacuum oven at 200 °C for 1 h to remove impurities before use [11, 12]. The ASC powder was mixed with a conducting support, carbon black, and poly(tetrafluoroethylene) (PTFE) resin binder in a mortar by 90:5:5 in mass ratio. Then the mixture was pressed by a roller-press to form a sheet with constant thickness. The resulting sheet was heated in a vacuum oven at 120 °C for 12 h, and then pressed at 100 kg cm^{-2} to form a disk electrode with a stainless-steel mesh current collector.

A mixture of ethylene carbonate and dimethyl carbonate (EC + DMC, 1:1 in volume) was used as the organic solvent of the electrolytic solution. The component solvents were Battery Grade (Kishida Chemical), and used as received without further purification. The water contents in the solvents were less than 20 ppm. The electrolytic salt mainly used was lithium hexafluorophosphate ($LiPF_6$, from Tomiyama Pure Chemical Industries), which was dissolved in the organic solvent with 1.0 mol dm^{-3} (M) concentration under a dry Ar atmosphere.

The electrochemical experiments were conducted using a conventional 3-electrode beaker cell. A Pt-sheet with high surface area and Ag wire in the same electrolyte solution were used as the auxiliary and quasi-reference electrodes (QRE), respectively. The electrochemical activation was carried out by potential scanning with 2.0 mV s^{-1} using a potentiostat (Hokuto Denko, HZ-3000) coupled with a personal computer. The potential limits for anodic and cathodic scans were properly chosen depending on the activation conditions. Constant-potential polarization was also employed for the activation process, whose details are individually described in the following section.

Specific surface area and pore-size distribution of the carbon material before and after the electrochemical activation were determined by N_2-adsorption/desorption isotherms using a surface area analyzer (Quantachrome NOVA2000). Morphological changes of ASC after the electrochemical treatments were monitored by a scanning electron microscope (SEM; Keyence, VE8800). Structure changes of the carbon material were examined by ex-situ X-ray diffraction (XRD; Rigaku, Ultima IV Protectus, Cu$K\alpha$ radiation). Ex-situ Raman spectroscopy was also employed to analyze the structural change in the carbon during the electrochemical activation. The measurement was carried out using a Raman spectrometer (JASCO, MRS-3000) with green-diode laser (532 nm) as an exciting source. Chemical shifts of the lithium species in the carbon material was determined by a solid-state ^{7}Li NMR spectrometer (JEOL, JNM-ECA500). The measurement was conducted at 25 °C using LiCl as a reference. In these experiments, the ASC electrode was activated by potential scanning or at constant-potential polarization, whose conditions will be described later in detail. The activated electrode was rinsed thoroughly with the component solvent, DMC, in a glove box filled with dry Ar, and then set to each sample holder without exposure to the atmosphere.

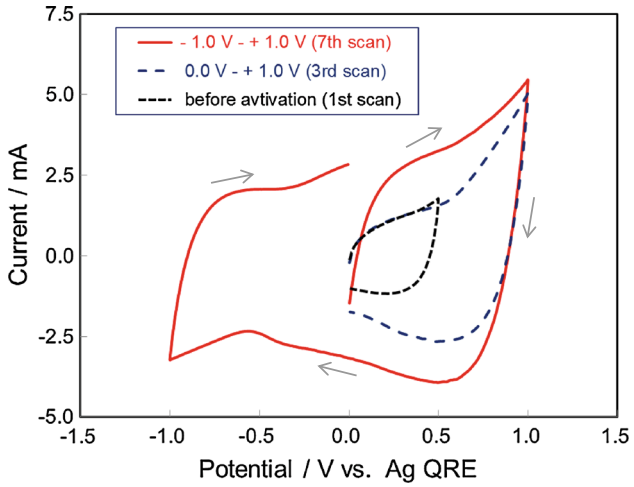

Fig. 1 Current–potential response during the electrochemical activation of ASC in 1.0 M $LiPF_6$ in EC + DMC (1:1). *Dotted line* before activation (1st scan), *Dashed line* from 0 to +1.0 V (3rd scan), *Solid line* from 0 to +1.0 V then to −1.0 V (7th scan), Potential scan rate: 2 mV s^{-1}

3 Results and discussion

The as-prepared sample ASC had an average particle size of ca. 10 μm, and specific surface area of 68 m^2 g^{-1} in its powder state. The specific surface area measured by BET method was reduced to about 30 m^2 g^{-1} after the process to form an electrode with carbon black conducting powder and a PTFE binder. Figure 1 shows typical current response of the ASC electrode during the electrochemical activation in 1.0 M $LiPF_6$/EC + DMC. In a narrow potential region between 0.0 and +0.5 V versus Ag QRE, the ACS electrode gave only small current response (1st scan in Fig. 1). However, it increased with the extention of

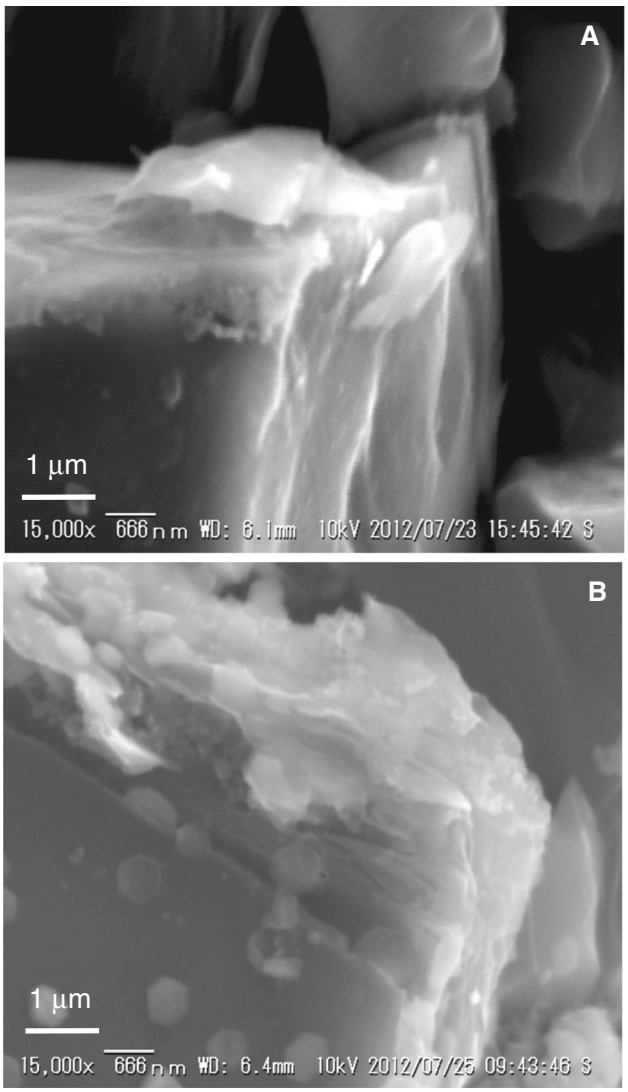

Fig. 2 SEM images of ASC particles **a** before and **b** after the electrochemical activation (20 cycles between −2.8 and +1.5 V versus Ag QRE in 1.0 M $LiPF_6$/EC + DMC (1:1)

the positive potential limit to +1.0 V, and after that higher capacitive current response was observed (3rd scan in Fig. 1). The current response was further increased with extending the potential limit to cathodic one, e.g., −1.0 V (7th scan in Fig. 1). The resulting ASC electrode, polarized in the potential range between −1.0 and +1.0 V, showed a much larger current response, whose rectangular shape is typical for non-faradaic capacitance behavior. We have called this type of current increase "Electrochemical Activation," which is apparently induced by anodic and/or cathodic polarization in organic electrolyte solutions. The current response after the electrochemical activation was dependent on the composition of the electrolyte solution, i.e., the combination of the electrolytic salt and the solvent. In this work, hereafter as a typical case,

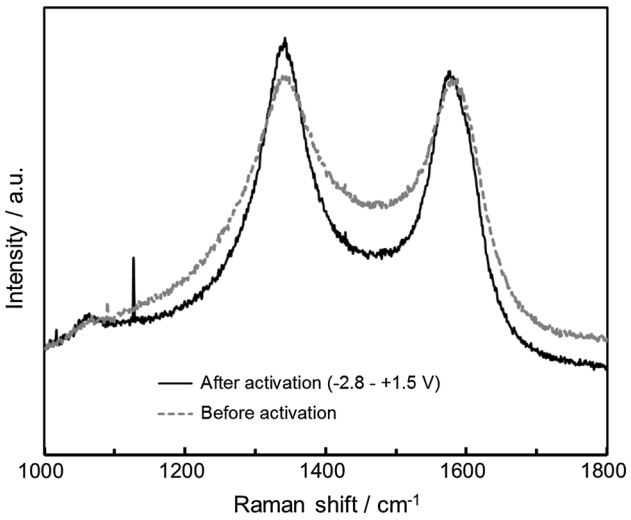

Fig. 3 Raman spectra of ACS before and after the electrochemical activation. *Dotted line* before activation, *Solid line* After the activation (between −2.8 and +1.5 V versus Ag QRE)

1.0 M $LiPF_6$/EC + DMC was used to investigate the detail of the electrochemical activation process.

Figure 2 shows SEM images of ASC before and after the electrochemical activation. Here the ASC electrode was treated under repeated potential cycling (20 times) between −2.8 and +1.5 V versus Ag QRE with a scan rate of 2.0 mV s^{-1} in 1.0 M $LiPF_6$/EC + DMC. The surface of pristine ASC particle (A: before activation) has smooth morphology. For the sample after the repeated potential cycling (B), the surface shows some exfoliation of graphene layers, especially at the edge part of the particle. This result strongly suggests that the electrochemical activation of ASC is accompanied by changes in the surface morphology.

Raman spectroscopy is a useful tool to characterize the nature of carbon materials for electrochemical uses [13, 14]. Figure 3 shows a comparison of Raman spectra for ASC samples before and after the electrochemical activation, in which the potential cycling was repeated 20 cycles between −2.8 and +1.5 V. The ASC sample shows two peaks in Raman shift that are typically observed for carbon materials having partly crystallized graphite sturcture, where the peaks around 1,360 and 1,560 cm^{-1} are called D- and G-bands, respectively [13]. These are generally assigned to sp^3 (D) and sp^2 (G) nature of carbon–carbon bonds, and its strength ratio (D/G) is used as a measure of the ordering of graphene layer stacking in the material. The electrochemical cycling tend to increase the intensity ratio of D/G, which implies some increments in the disordered structure. However, no visible peak shifts were detected, which was somewhat different from the previously reported case for the activation of hard carbon [14]. From these results, we can speculate that the electrochemical

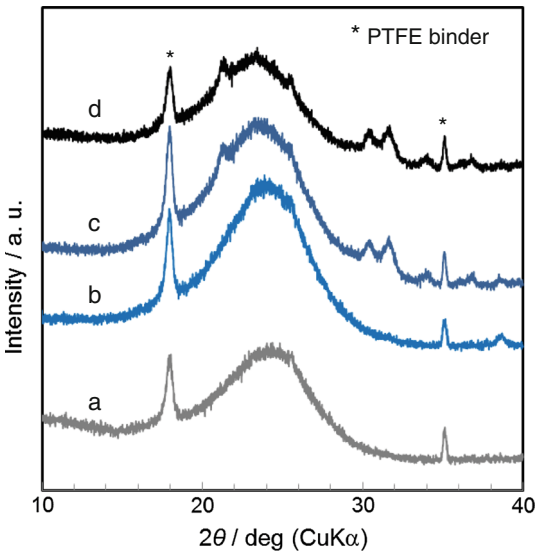

Fig. 4 XRD patterns of ASC electrode *a* before and *b–d* after the electrochemical activation in 1.0 M $LiPF_6$/EC + DMC (1:1). *b* from 0 to −1.5 V, *c* from 0 to −2.8 V, 0064 from 0 to +1.5 V and then to −2.8 V

activation of ASC is strongly associated with somewhat destruction of graphite structure inside the carbon material.

Figure 4 indicates the changes in XRD pattern of ASC by the electrochemical activation under different conditions in $LiPF_6$/EC + DMC. In this experiment, the sample electrode was activated by potential scanning from 0 to −1.5 V (curve b), from 0 to −2.8 V directly (curve c), or from 0 to +1.0 V and then to −2.8 V (curve d) with a scan rate of 2.0 mV s^{-1}. The XRD pattern of the pristine ASC gives a broad diffraction peak at around $2\theta = 25°$, which reveals that the material consists of small crystallites of graphite structure. The average lattice constant was calculated to be 0.371 nm for pristine ASC. We can observe peak shifts to lower angle for the sampe activated by cathodic polarization in $LiPF_6$/EC + DMC. The degree in peak shift depended on the activation condition. The sample polarized to more negative potential gave lower angle of the diffraction peak. Those diffraction peaks correspond to the average lattice parameters of 0.380 and 0.392 nm for the samples polarized to −1.5 V (curve b) and −2.8 V (curves c and d), respectively. These observations lead to qualitative discussion on the ion (Li^+) insertion during the electrochemical activation. That is, possible insertion of ionic species inside the carbon material would cause expansion of the graphite structure of ASC.

Chemical states of Li species incorporated in carbon materials have been widely discussed by means of solid-state ^{7}Li NMR, especially in lithium-ion battery technology [15–21]. Figure 5 shows ex-situ ^{7}Li NMR spectra of the carbon materials after the cathodic polarization in $LiPF_6$/EC + DMC. In Fig. 5a, ^{7}Li NMR spectrum for lithiated graphite is shown for comparison. The Li species in a graphite-intercalation compound (GIC) gives a sharp chemical shift around 46 ppm, which corresponds to partially charged Li immobilized at inter-layer of graphene sheets of the graphite crystal [15, 16], whose process is generally defined as "intercalation." As the graphite electrode was polarized potentiostatically at −10 mV versus Li/Li^+ reference electrode, an additional sharp peak corresponding to the deposition of metallic Li was also observed at about 260 ppm (not shown in Fig. 5, spectrum a). On the other hand, the ASC cathodically polarized at −2.8 V versus Ag QRE showed no sharp signal at 46 ppm, but broad peak around 30 ppm (Fig. 5, spectra b and c). With respect to the Li^+ species adsorbed at or incorporated in narrow space of pore structures, chemical shifts around 0 ppm were reported in literature [18, 20]. Also, for the Li^+ insertion in hard carbon materials, it was found that gradual changes in the chemical shift can be observed with the increase in the doping level [17–19, 21]. Here, the "insertion" process occuring at narrow space of disordered carbon structure is clearly distinguished from the "intercalation" of ions to form GIC compounds. Thus, the present results strongly suggest that the incorporated Li species in ASC by cathodic polarization has a different circumstance from that in GIC, as shown in spectrum a, not but simply adsorbed ion observed for conventional activated carbon. Since the ionicity of Li species tends to be high with the higher magnetic field (lower chemical shift with respect to free Li^+ at 0 ppm) [18], the observed chemical shifts around 20–50 ppm clearly indicate that the electrochemical activation of ASC should be associated with ion (Li^+) insertion (not intercalation) inside the bulk of carbon, as already discussed by different research groups [7, 8, 14].

Figure 6a shows N_2-adsorption/desorption ithothems for the pristine ASC and electrochemically activated ASC. In these experiments, the activation was conducted by repeated potential scanning with different potential limits, −1.0 to +1.0 V (curve b) and −1.5 to +1.5 V (curve c). Specific surface area of each electrode was estimated by BET method using desorption branch of the isotherm. As the ASC powder was once molded to a electrode sheet with PTFE binder, the specific surface area was reduced to 27 m^2 g^{-1} even for the material before the electrochemical treatment. This is probably because the micropores in the carbon material could not respond to the N_2-adsorption after the electrode preparation. However, it was clear that the electrochemical activation causes the increase in the BET surface area to 40 and 96 m^2 g^{-1} for the activation conditions with potential limits of −1.0 to +1.0 V and −1.5 to +1.5 V, respectively. In Fig. 6b, the pore-size distribution calculated by BJH method is compared for the electrodes before and after the electrochemical activation.

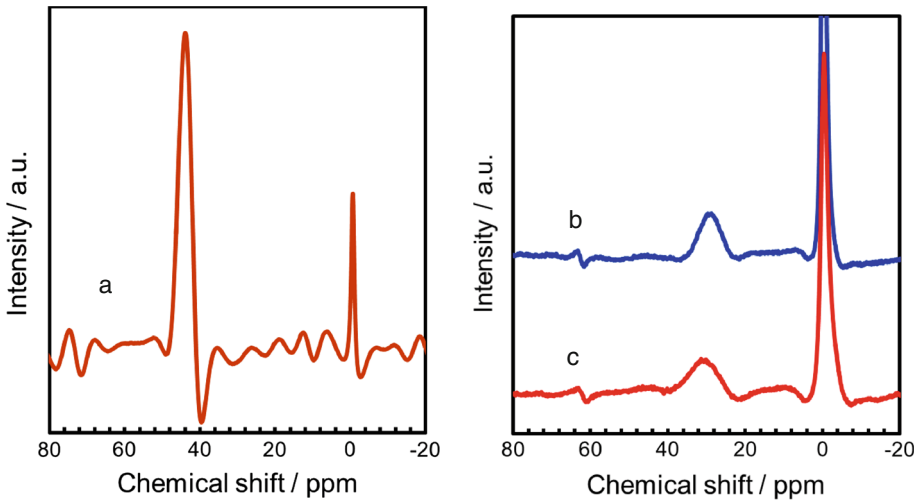

Fig. 5 ^{7}Li NMR spectra for *a* lithiated graphite and *b*, *c* electrochemically activated ASC. *a* lithiated at −10 mV versus Li/Li^{+} in 1.0 M $LiPF_6$/EC + DMC (1:1), *b* polarized at −2.8 V versus Ag QRE in 1.0 M $LiPF_6$/EC + DMC (1:1), *c* polarized at +1.5 V and then at −2.8 V versus Ag QRE in 1.0 M $LiPF_6$/EC + DMC (1:1)

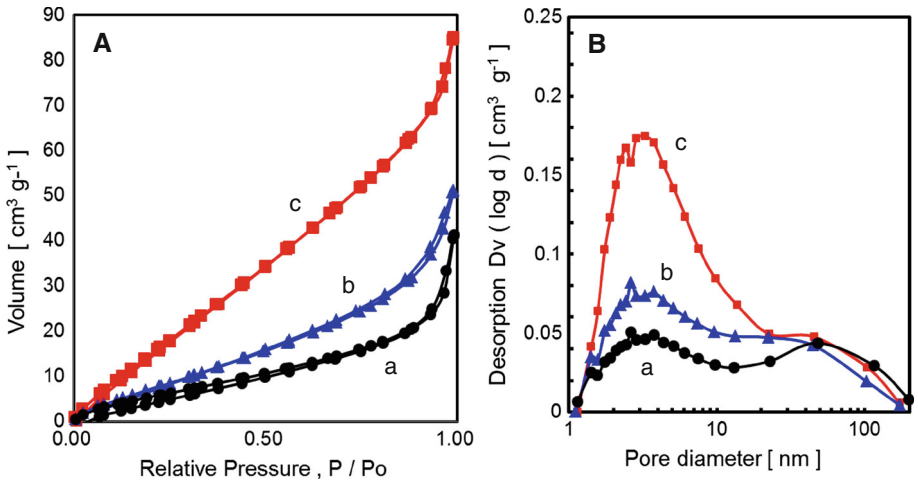

Fig. 6 **a** Adsorption/desorption isotherms and **b** pore-size distribution of ASC **a** before electrochemical activation and **b**, **c** after the electrochemical activation in 1.0 M $LiPF_6$/EC + DMC (1:1). Activation condition: **b** −1.0 to +1.0 V versus Ag QRE, **c** −1.5 to +1.5 V versus Ag QRE

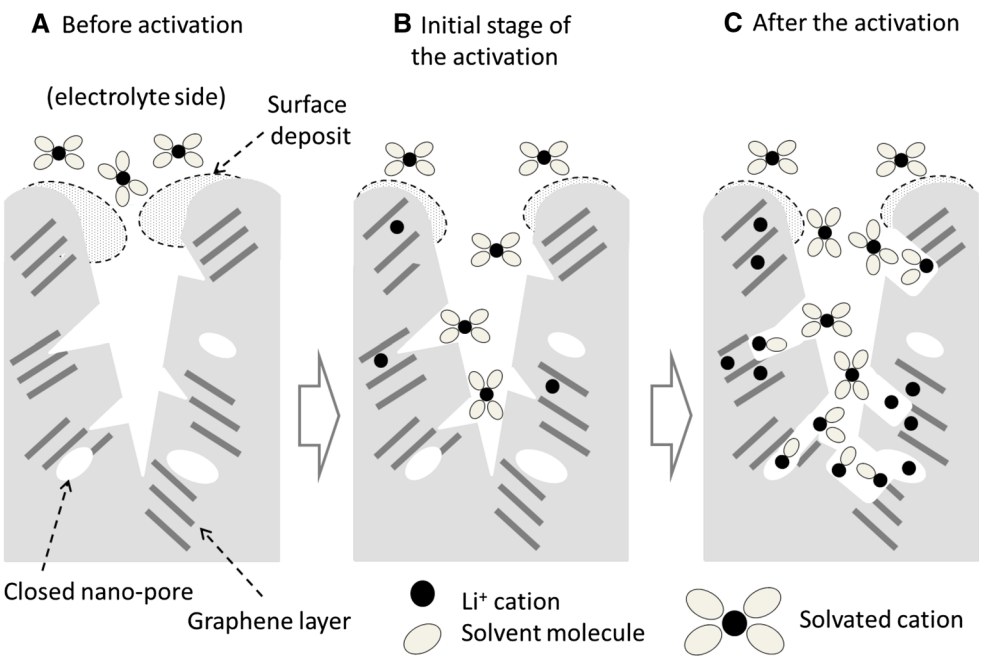

Fig. 7 A schematic model for electrochemical (cathodic) activation of ASC in $LiPF_6$/EC + DMC solution. (Anionic species are not shown for avoiding complexity)

As the material was once formed into an electrode sheet using PTFE binder, we can find very small contribution of micropore structure (pore diameter, $d < 2$ nm) for every sample. On the other hand, the contribution of mesopore region ($2 \leq d < 50$ nm) became more significant after the potential cycling, whose extent depended on the cycling condition. These changes in the specific surface area and the pore-size distribution would correspond qualitatively to the increase in the non-faradaic capacitive curent for ASC after the electrochemical treatment.

From above observations, we propose a scheme for the electrochemical activation of ASC in organic electrolyte solutions (Fig. 7).

(1) The pristine ASC particle is partly covered with surface deposit, which was formed during the carbonization process of the material and will prevent the ions from accessing the inner space of the carbon structure [6, 10] (a: Before activation).
(2) The electrochemical (cathodic) polarization induces accumulation of ions (cation) at the electrode/electrolyte interface to compensate the charge at the carbon surface.
(3) Electrochemical insertion of ions into the inter-layer of graphite structure or free nano-space of disordered carbon structure causes the exfoliation of the surface (not included in the model shown in Fig. 7) and expansion of the inner space of the carbon material (b: Initial stage of the activation).
(4) The repeated potential cycling accompanied by electrochemical insertion/desertion of ions results in the increase in the number of ion-accessible site inside the carbon material (c: After the activation), which would be reflected by the increase in the specific surface area and changes in the pore-size distribution evaluated by N_2-adsorption ithotherms.

These processes cause some increase in the volume of the material, and hence decrease in the density of the material. Even if such volumetric change occurs, the ASC electrode shows high specific capacity per volume (F L^{-1}) after the electrochemical polarization treatments.

4 Conclusion

The electrochemical activation process of ASC in an organic electrolyte solution was investigated by means of SEM observation, ex-situ Raman, XRD, and ^{7}Li NMR measurements. The cathodic polarization in $LiPF_6$/EC + DMC electrolyte solution causes the morphological and structural changes of the carbon material. The pore-size distribution evaluated by N_2-adsorption/desorption isotherms for ASC electrodes before and after the activation indicated that the pore structure becomes developed after the electrochemical polarization, especially in the pore-diameter range of 2–10 nm. A schematic model, which includes the electrochemical insertion of ions into the carbon material, was proposed for the mechanism of the electrochemical activation of ASC.

References

1. Kötz R, Carlen M (2000) Principles and applications of electrochemical capacitors. Electrochim Acta 45:2483–2498
2. Centeno TA, Hahn M, Fernández JA, Kötz R, Stoeckli F (2007) Correlation between capacitances of porous carbons in acidic and aprotic EDLC electrolytes. Electrochem Commun 9:1242–1246. doi:10.1016/j.elecom.2007.01.031
3. Lin R, Huang P, Ségalini J, Largeot C, Taberna PL, Chimiola J, Gogotsi Y, Simon P (2009) Solvent effect on the ion adsorption from ionic liquid electrolyte into sub-nanometer carbon pores. Electrochim Acta 54:7025–7032. doi:10.1016/j.electacta.2009.07.015
4. Laheäär A, Jänes A, Lust E (2011) Electrochemical properties of carbide-derived carbon electrodes in non-aqueous electrolytes based on different Li-salts. Electrochim Acta 56:9048–9055. doi:10.1016/j.electacta.2011.05.126
5. Gogotsi Y (2013) Zero- to Three-Dimensional Carbon-Based Nanomaterials for Capacitive Energy Storag. Extended Abstract of 2013 International Conference on Advanced Capacitors (ICAC2013, Osaka), PL02
6. Takeuchi M, Koike K, Maruyama T, Mogami A, Okamura M (1998) Electrochemical intercalation of tetraethylammonium tetrafluoroborate into KOH-treated carbon consisting of multi-graphene sheets for an electric double layer capacitor. Electrochemistry 66:1311–1317
7. Takeuchi M, Maruyama T, Koike K, Mogami A, Oyama T, Kobayashi H (2001) Non-porous carbon for a high energy density electric double layer capacitor. Electrochemistry 69:487–492
8. Mitani S, Lee SI, Saito K, Yoon SH, Korai Y, Mochida I (2005) Activation of coal tar derived needle coke with K_2CO_3 into an active carbon of low surface area and its performance as unique electrode of electric double-layer capacitor. Carbon 43:2960–2967. doi:101016/j.carbon.2005.05.047
9. Kim IJ, Yang S, Jeon MJ, Moon SI, Kim HS, Lee YP, An KH, Lee YH (2007) Structures and electrochemical performances of pyrolized carbons from graphite oxides for electric double-layer capacitor. J Power Sources 173:621–625. doi:101016/j.jpowsour.2007.07.042
10. Aida T, Murayama I, Yamada K, Morita M (2007) High-energy-density hybrid electrochemical capacitor using graphitizable carbon activated with KOH for positive electrode. J Power Sources 166:462–470. doi:101016/j.jpowsour.2007.01.037
11. Ohta T, Kim IT, Egashira M, Yoshimoto N, Morita M (2012) Effects of electrolyte composition on the electrochemical activation of alkali-trated soft carbon as an electric double-layer capacitor electrode. J Power Sources 198:408–415. doi:101016/j.jpowsour.2011.10.006
12. Kim IT, Egashira M, Yoshimoto N, Morita M (2012) Combination of alkali-treated soft carbon and activated carbon fiber electrodes for asymmetric electric double layer capacitor. Electrochemistry 80: 415–420. doi:10.5796/electrochemistry.80.415

13. Ferrari AC (2007) Raman spectroscopy of graphene and graphite: disorder, electron-phonon coupling and nanodiabatic effects. Solid State Commun 143:47–57. doi:10.1016/j.ssc.2007.03.052
14. Hardwick LJ, Ruch PW, Hahn M, Scheifele W, Kötz R, Novák P (2008) In situ Raman spectroscopy of insertion electrodes for lithium-ion batteries and super capacitors: first cycle effects. J Phys Chem Solids 69:1232–1237. doi:10.1016/j.jpcs.2007.10.017
15. Zaghib K, Tasumi K, Abe H, Ohsaki T, Sawada Y, Higuchi S (1995) Electrochemical behavior of an advanced graphite whisker anodic electrode for lithium-ion rechargeable batteries. J Power Sources 54:435–439
16. Tatsumi K, Kawamura T, Higuchi S, Hosotsubo T, Nakajima H, Sawada Y (1997) Anode characteristics of non-graphitizable carbon fibers for rechargeable lithium-ion batteries. J Power Sources 68:263–266
17. Ago H, Tanaka K, Yamabe T, Takegoshi K, Terao T, Yata S, Hato Y, Ando N (1997) ^{7}Li NMR study of Li-doped polyacenic semiconductor (PAS) materials. Synth Met 89:141–147
18. Łoś S, Letellir M, Azaïs P, Duclaux L (2006) Li doped carbons (activated microporous carbons and graphite): charcaterisation by resonance spectroscopies (ESR and ^{7}Li NMR) and their potentiality for hydrogen adsorption. J Phys Chem Solids 67:1182–1185. doi:10.1016/j.jpcs.2006.01.092
19. Gotoh K, Maeda M, Nagai A, Goto A, Tansho M, Hashi K, Shimizu T, Ishida H (2006) Properties of a novel hard-carbon optimized to large size Li ion secondary battery studied by ^{7}Li NMR. J Power Sources 162:1322–1328. doi:10.1016/j.jpowsour.2006.09.001
20. Eom JY, Kwon HS (2011) Effects of the chemical etching of single-walled carbon nanotubes on their lithium storage properties. Mater Chem Phys 126:108–113. doi:10.1016/j.matchemphys.2010.11.060
21. Hori H, Shikano M, Kobayashi H, Koike S, Sakaebe H, Saito Y, Tasumi K, Yoshikawa H, Ikenaga E (2013) Analysis of hard carbon for lithium-ion batteries by hard X-ray photoelectron spectroscopy. J Power Sources 242:844–847. doi:10.1016/j.jpowsour.2013.05.160